



**HAL**  
open science

# Guidelines for data-driven approaches to study transitions in multiscale systems: The case of Lyapunov vectors

Akim Viennet, Nikki Vercauteren, Maximilian Engel, Davide Faranda

## ► To cite this version:

Akim Viennet, Nikki Vercauteren, Maximilian Engel, Davide Faranda. Guidelines for data-driven approaches to study transitions in multiscale systems: The case of Lyapunov vectors. *Chaos: An Interdisciplinary Journal of Nonlinear Science*, 2022, 32, pp.113145. 10.1063/5.0093804 . hal-03626146v2

**HAL Id: hal-03626146**

**<https://hal.science/hal-03626146v2>**

Submitted on 14 Nov 2022

**HAL** is a multi-disciplinary open access archive for the deposit and dissemination of scientific research documents, whether they are published or not. The documents may come from teaching and research institutions in France or abroad, or from public or private research centers.

L'archive ouverte pluridisciplinaire **HAL**, est destinée au dépôt et à la diffusion de documents scientifiques de niveau recherche, publiés ou non, émanant des établissements d'enseignement et de recherche français ou étrangers, des laboratoires publics ou privés.

1 **Guidelines for data-driven approaches to study transitions in multiscale systems: the**  
2 **case of Lyapunov vectors**

3 Akim Viennet,<sup>1, a)</sup> Nikki Vercauteren,<sup>2, b)</sup> Maximilian Engel,<sup>3, c)</sup> and Davide Faranda<sup>4, d)</sup>

4 <sup>1)</sup>*Department of Physics, Ecole Normale Supérieure, 75005 Paris,*  
5 *France*

6 <sup>2)</sup>*Department of Geosciences, University of Oslo, 0371 Oslo,*  
7 *Norway*

8 <sup>3)</sup>*Institute of Mathematics, Freie Universität, 14195 Berlin,*  
9 *Germany*

10 <sup>4)</sup>*Laboratoire des Sciences du Climat et de l'Environnement,*  
11 *UMR 8212 CEA-CNRS-UVSQ, Université Paris-Saclay, IPSL,*  
12 *91191 Gif-sur-Yvette, France*

13 (Dated: 14 November 2022)

14 We study in detail the role of covariant Lyapunov vectors and their respective an-  
15 gles for detecting transitions between metastable states in dynamical systems, as  
16 recently discussed in several atmospheric science applications. The underlying mod-  
17 els are built from data by the dynamical clustering method, called FEM-BV-VAR,  
18 and the Lyapunov vectors are approximated based on these models. We test this  
19 data-based numerical approach at the hand of three well-understood example sys-  
20 tems with increasing dynamical complexity, identifying crucial properties that allow  
21 for a successful application of the method: in particular, it turns out that the method  
22 requires a clear multiple time scale structure with fast transitions between slow sub-  
23 systems which can be dynamically characterized by invariant neutral directions of  
24 the linear approximation model.

---

a) akim.viennet@gmail.com

b) nikki.vercauteren@geo.uio.no

c) maximilian.engel@fu-berlin.de

d) davide.faranda@lsce.ipsl.fr; also at London Mathematical Laboratory, 8 Margravine Gardens London, W6 8RH, UK; and also at LMD/IPSL, Ecole Normale Supérieure, PSL research University, Paris, France

25 In climate science, systems with multiple metastable states are ubiquitous. In  
26 non-equilibrium systems with a non-stationary but steady forcing or intrinsic  
27 noisy dynamics, metastability denotes an intermediate energetic state other than  
28 the system's state of least energy: the fluctuations in the forcing parameter or  
29 in the dynamics can enable the system to reach metastable states and stay there  
30 for a finite amount of time, then leaving into another regime before coming back  
31 with a positive probability. Knowing their stability properties and the probability  
32 of transitioning from one state to another is of great help to understand and pre-  
33 dict the dynamics of such systems. Many tools have been developed to address  
34 this challenge, among which covariant Lyapunov vectors have proven to be very  
35 useful. The numerical calculation of these vectors generally requires an a priori  
36 knowledge of the set of equations governing the dynamics, and therefore cannot  
37 be applied directly to experimental data. However, recent purely data-driven  
38 methods have been developed to estimate the covariant Lyapunov vectors. Our  
39 study aims to identify the crucial conditions under which a data-driven factor  
40 model approach can successfully estimate the alignment of covariant Lyapunov  
41 vectors to predict critical transitions. To this end, we discuss in detail the FEM-  
42 BV-VAR approach for multiscale systems and test the method on three systems  
43 of increasing dynamic complexity, including two explicit classical models and  
44 experimental data for turbulent flow. As the tested method is expected to be  
45 relevant in a wide range of climate science applications, our key contribution is  
46 to show under which circumstances reliable results can be expected.

---

## 47 I. INTRODUCTION

48 Dynamical systems theory deals with the prediction of trajectories of natural systems  
49 originating by one given or a set of initial conditions. This task is particularly challenging  
50 when the system is chaotic and even more when the system features several metastable  
51 states or multiscale features<sup>1,2</sup>. Among all the possibilities, here we focus on the stability  
52 properties of certain meta-stable states, that organize the phase space, and the estimation  
53 of the probability of switching from one state to another. Many mathematical tools have

54 been developed to address those questions, one of them being the study of the so-called  
55 *covariant Lyapunov vectors* (CLVs) (also known as Oseledets vectors), and the associated  
56 *Lyapunov exponents* (LEs). These vectors give a basis on the tangent space at points of  
57 trajectories, providing directions of linear perturbation growth along the dynamics<sup>3-5</sup>. They  
58 can be seen as a generalization of the linear stability theory for fixed points and of Floquet's  
59 theory for limit cycles, since Lyapunov vectors and exponents can be computed along any  
60 trajectory of a smooth dynamical system. The CLVs give the directions of growth or decay  
61 of a perturbation, and the LEs give the associated rate of asymptotic growth or decay. An  
62 increase of one of the unstable LEs has been associated to a higher instability for various  
63 theoretical and physical systems<sup>6,7</sup>.

64 In many cases, transient (chaotic) behavior cannot be detected by asymptotic LEs which  
65 average out transient dynamics via ergodic limits; hence, *finite-time Lyapunov exponents*  
66 (FTLEs) are often more suitable to capture the degree of uncertainty at different points of  
67 trajectories and their small neighbourhoods.

68 The directions of unstable CLVs indicate the directions towards which an error will grow  
69 with the rates given by the associated (FT)LEs. For example, this tool can be used in  
70 ensemble weather forecasting to identify how to enforce initial perturbations to optimally  
71 span the space of possible realizations of the weather<sup>8</sup>. Another quantity of interest is the  
72 angle between the flow direction and the most unstable CLV. An alignment of those vectors  
73 has been used as a predictor for transitions, tipping points or catastrophes (extreme events)  
74 in several systems<sup>9-11</sup>. In particular, this criterion has been proven to be an important early-  
75 warning sign for abrupt transitions in the Peña and Kalnay climate toy-model<sup>12</sup>. Finally,  
76 Quinn et al.<sup>13</sup> suggested that the projection of the most unstable CLV just before a transition  
77 between two states could inform on the patterns that triggered the instability and then the  
78 transition.

79 Summarizing, the computation of CLVs and associated LEs is of high interest for the  
80 analysis of dynamical systems. Recent progress was made to compute them numerically,  
81 due to various algorithms by Ginelli et al.<sup>4</sup>, Wolfe and Samelson<sup>5</sup>, and Froyland et al.<sup>14</sup>.  
82 However, all those algorithms rely on the knowledge of an analytic expression of the model,  
83 in order to differentiate the flow and compute the linear cocycles (see Section II B for an  
84 introduction to those methods). This suggests that it is rather difficult to use such methods  
85 based on observations for which the underlying model is unknown or only partially known,

86 such as reanalysis atmospheric data.

87 Yet, recent progress has been made to estimate CLVs from data series. Lately, Martin  
88 et al.<sup>15</sup> suggested to use sparse identification of non-linear dynamics to infer the Jacobian  
89 matrices from trajectories. Quinn et al.<sup>13</sup> recently introduced another method to compute  
90 CLVs directly from data, aimed at dealing with systems with stochastic transitions. This  
91 latter method will be studied and tested in this paper. It relies on fitting a model to  
92 the observations via a dynamical, or model-based clustering method initially introduced by  
93 Horenko<sup>16,17</sup>: the FEM-BV-VAR (Finite Element clustering with bounded variation (FEM  
94 BV) vector autoregressive (VAR)) clustering approach. Differently from more classical,  
95 geometrical clustering methods, in this framework a state is not defined by a geometrical  
96 area in the phase space, but by an estimated auto-regressive dynamics (see Section III A  
97 for details). The whole system is then switching between those dynamical models. This  
98 method is particularly adapted to the purpose since it provides not only a cluster affiliation  
99 sequence, but also a linear (auto-regressive) model for each of the states. One can then  
100 use these (approximated) models to compute an approximation of the CLVs and of the LEs  
101 for the dynamical system underlying the data, and thus get some insights on the stability  
102 of the states and of the stable and unstable directions. Quinn et al.<sup>13</sup> used this approach  
103 to analyse the dynamics of atmospheric circulation patterns in the northern hemisphere.  
104 They investigated the dynamical stability properties of recurrent and persistent states of  
105 the atmospheric circulation patterns or regimes known as the North Atlantic Oscillation  
106 (NAO) and atmospheric blocking events. In particular, the CLVs were used to analyse  
107 the pressure distribution patterns related to transitions between the recurrent circulation  
108 regimes, leading to insightful observations since weather forecasting and climate models  
109 struggle to capture the onset and decay of blocking events.

110 These results led to the question whether the method is applicable for other systems of  
111 interest and to which extent it more generally captures relevant information on the dynam-  
112 ics. The aim of this work is to explore this question by testing the method in several systems  
113 for which some a priori knowledge of the CLVs and of the transitions between regimes is  
114 available: a fast-slow FitzHugh-Nagumo oscillator, a well-studied Von Kármán turbulent  
115 flow from a laboratory experiment, and a Lorenz 63 system, where the order of our presen-  
116 tation follows an increase of dynamical complexity. Results on those different systems will  
117 show that the method provides several insights on the dynamics, quantifying the stability of

118 different (meta-stable) states and thereby identifying transitions between them. This holds  
119 true in particular for the Von Kármán flow. However, we also demonstrate why such con-  
120 clusions may be treated with caution, considering the strong dependence on the existence of  
121 an dynamically invariant normal tangent flow direction, a visible time scale separation and  
122 a large number of hyper-parameters.

123 In this paper, we will first present the details of the method that allows one to compute  
124 approximated CLVs from a data series. Then we will try to assess its validity, by applying  
125 it on a FitzHugh-Nagumo oscillator, experimental data from the Von Kármán flow and the  
126 Lorenz 63 model. Finally, we will discuss the scope of the methods at the hand of these  
127 examples, illustrating its potential but also several caveats for its application.

## 128 II. THE LYAPUNOV VECTORS AND THEIR NUMERICAL 129 COMPUTATION

### 130 A. Mathematical background

131 Let us first introduce the notion of CLVs. They arise from a non-autonomous general-  
132 ization of the linear stability analysis at fixed points and Floquet theory at limit cycles to  
133 any point of the trajectory. For a dynamical system, the CLVs form a basis of the tangent  
134 space and give the directions of growth or decay of any perturbation around a background  
135 flow. The Lyapunov exponents (LEs) give the associated rate of growth or decay (see Fig.1).  
136 Assuming ergodicity of a dynamical system  $\Phi_t(x_0)$ , whose trajectories we will simply denote  
137 by  $x(t)$ , one observes that the LEs are global numbers that characterise the whole attrac-  
138 tor, whereas the CLVs may depend on the particular points of the trajectory (but are still  
139 asymptotic objects).

In more detail, the existence of Lyapunov exponents with corresponding directions on  
the tangent space is given by Oseledets' Multiplicative Ergodic Theorem (MET)<sup>18</sup>. Under  
a mild integrability condition with respect to an ergodic invariant measure, this theorem  
gives us, in each point of the trajectory, the existence of a splitting of the tangent space into  
 $p \leq d$  subspaces

$$\mathbb{R}^d = Y_1(x(t)) \oplus \cdots \oplus Y_p(x(t)),$$

140 such that for all  $v \in Y_i(x(t))$ ,

$$\lim_{\tau \rightarrow \infty} \frac{1}{\tau} \log \|\mathcal{F}(t, t + \tau) \cdot v\| = \lambda_i, \quad (1)$$

where  $\mathcal{F}$  denotes the linear propagator for the tangent flow, i.e.

$$\mathbf{v}(t_2) = \mathcal{F}(t_1, t_2) \mathbf{v}(t_1)$$

141 and  $\lambda_1 > \lambda_2 > \dots > \lambda_p$  are the distinct LEs with multiplicities  $m_i \geq 1$ ,  $i = 1, \dots, p$ . The  
 142 CLVs  $v_i^j(t)$ ,  $j = 1, \dots, m_i$ , are then representative vectors from the Oseledets subspaces  
 143  $Y_i(x(t))$ , which are unique up to scalar factors if  $m_i = 1$  and chosen as a set of  $m_i$  linearly  
 144 independent vectors in  $Y_i(x(t))$  otherwise. Let us order them as  $\phi_k$ ,  $k = 1, \dots, d$ , where  
 145  $v_1^1 = \phi_1, \dots, v_1^{m_1} = \phi_{m_1}$ , and so on (see also Figure 1 where all  $m_i = 1$  as will be the case in  
 146 our examples).

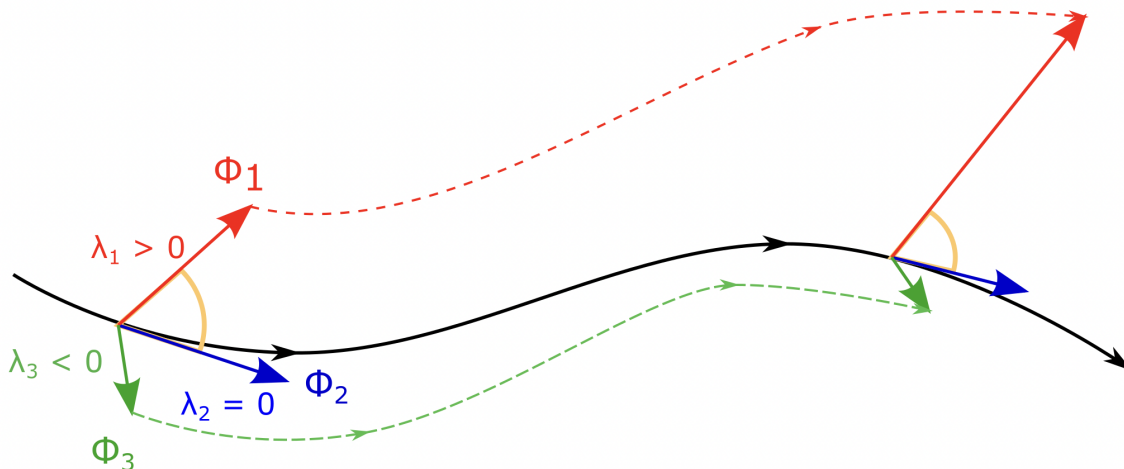


FIG. 1: Contraction and expansion of CLVs along a trajectory with positive, negative and zero Lyapunov exponent  $\lambda_i$ ,  $i = 1, 2, 3$ . In this setting, we have at each point three CLVs ( $\phi_1$ ,  $\phi_2$  and  $\phi_3$ ). The solid line represents the unperturbed trajectory, while the dotted lines represent the perturbed trajectories, along the stable (in green) and the unstable (in red) directions. The so-called alignment  $\theta_{12}$  is given by the cosine of the orange angle.

147

148

149 As described in Section I, LEs and CLVs give important information on the stability  
 150 properties of the dynamics, and have been used to predict transitions and extreme events.  
 151 One key quantity is the angle between the neutral CLV (the CLV associated with a zero LE,

152 which is always tangent to the flow direction) and the most unstable CLV (the one associated  
 153 with the largest positive LE), given that they both exist. Let us call  $\theta_{ij}$  the cosine of the  
 154 angle between the CLVs  $\phi_i$  and  $\phi_j$ :

$$\theta_{ij}(t) = \frac{|\phi_i(t) \cdot \phi_j(t)|}{\|\phi_i(t)\| \|\phi_j(t)\|} \quad (2)$$

155 Many studies suggest that, for  $\phi_i$  representing the most unstable direction and  $\phi_j$  a neutral  
 156 direction, this angle is related to the probability of transitions between characteristic states:  
 157 the more these two vectors align, the higher such a switching probability is expected to  
 158 be. Sharafi et al.<sup>9</sup> have applied this criterion to various fast-slow systems, whereas Beims  
 159 et al.<sup>10</sup> have used it to predict extreme events in a Rössler oscillator. In the following, we  
 160 will call “alignment of CLVs” the absolute value of the cosine of the angle between a most  
 161 unstable CLV and a neutral one. In cases without a neutral direction, one may take the  
 162 CLV associated with the Lyapunov exponent closest to 0 and consider this direction as a  
 163 *near-neutral* one (see also Section IV C).

164 Note that the CLVs and associated Lyapunov exponents are asymptotic objects whereas  
 165 the transitions we are interested in happen on finite time scales and the analyzed time series  
 166 are also naturally finite. Hence, in reality one analyzes *Finite Time Lyapunov Exponents*  
 167 (FTLEs) which are defined analogously for a given finite  $\tau$  in Eq.(1), depending on space and  
 168 time. FTLEs associated to CLVs (or their finite time approximations one may also regard to  
 169 as Finite Time Lyapunov vectors (FTLVs)) may change their signs depending on  $\tau$ . In some  
 170 cases, there can exist strictly positive FTLEs even though the trajectory is asymptotically  
 171 stable (i.e. all LEs are negative). This is typical for globally asymptotically stable systems  
 172 with transient chaos. In particular, an asymptotically stable (or unstable) CLV might be  
 173 referred to as an unstable (or stable) CLV on certain finite time scales. Hence, we will call  
 174 CLVs stable or unstable in our numerical studies based on the local stability within the  
 175 investigated finite time scales. The FitzHugh-Nagumo oscillator discussed below exemplifies  
 176 this: while the trajectories asymptotically approach a stable periodic orbit (one negative,  
 177 one neutral LE), the CLVs and associated FTLEs can detect the local instability along the  
 178 fast subsystem (see Section IV A for further explanations). Generally speaking, FTLEs can  
 179 be used as a measure for the predictability of the local dynamics: the higher the largest  
 180 FTLE, the lower the predictability on the respective time scale (see, for example, Deremble



181 et al.<sup>19</sup> for the classical Lorenz 63 attractor and a one-layer quasi-geostrophic atmospheric  
 182 model). As suggested by Quinn et al.<sup>13</sup> (and before by Deremble et al.<sup>19</sup>), the time length  
 183  $\tau$  acts as a scale filter for the dynamics: with small  $\tau$  the computed FTLEs and the related  
 184 CLVs (or FTLVs) give insights on the short scale processes, whereas with larger  $\tau$  we get  
 185 closer and closer to asymptotic properties.

## 186 B. Direct computation of the CLVs

187 There exist several algorithms to numerically compute the CLVs. One of the most famous  
 188 methods was developed in 2007 by Ginelli et al.<sup>4</sup>. However, here we will use a modified  
 189 approach introduced in 2013 by Froyland et al.<sup>14</sup> (algorithm 2.2 in this reference). This  
 190 choice is motivated empirically by a faster convergence and by more consistent results in the  
 191 considered setting, when compared to results obtained with Ginelli’s algorithm.

The *Froyland algorithm* relies on a singular value decomposition of the forward cocycles starting at past fibers, then propagating the obtained orthogonal directions into covariant ones. Thus, computing the CLVs at a given point on the trajectory requires a pullback procedure from the past to the present (and beyond). This involves a number of time steps  $N$  for going to the past and a number of time steps  $M$  corresponding with the time length  $\tau$  in Eq. (1). In this study, for simplicity we always take  $M = N$  (as suggested in Froyland’s article and validated empirically). In theory, increasing  $N$  and  $M$  improves the approximation. However, our results show that convergence may fail due to the accumulation of numerical errors. Therefore,  $N$  and  $M$  are key parameters that act as a scale filter, similarly to  $\tau$  in the previous subsection. Another internal parameter to be adapted is given by the number of correction steps  $n$  for obtaining the covariant out of singular directions; for details see algorithm 2.2 in Froyland et al.<sup>14</sup>. To sum up, this algorithm requires to set three parameters:

$$M, N \text{ and } n$$

192 with, in this study,  $N = M$ .

193 Finally, let us emphasise that this algorithm requires an explicit expression for the lin-  
 194 ear propagator at each point. For continuous-time systems  $\dot{x} = f(t, x)$ , the linear prop-  
 195 agator solves the variational linear differential equation with matrix generator  $J(x, t) :=$   
 196  $(D_x f)(t, x)$ , i.e. the Jacobian of the vector field  $f$ . For discrete-time systems  $x_{n+1} = g(x_n)$ ,

197 the propagator is the product of the matrices  $A_n = (D_x g)(x_n)$ . Hence, computing the quan-  
 198 tities directly from data, for which the propagator is not known a priori, is out of reach.  
 199 The aim of this article is to investigate the capabilities of the above-mentioned Froyland’s  
 200 algorithm for computing approximate CLVs directly from observed time series, relying on  
 201 a prior modelling step using a model-based clustering framework. We hence explore, based  
 202 on systems of different complexity, the conditions under which the method first introduced  
 203 in<sup>13</sup> provides reliable results.

### 204 III. DYNAMICAL CLUSTERING METHOD

#### 205 A. FEM-BV-VAR approach

206 In the literature, various approaches address the problem of identifying persistent states  
 207 based on data. They can be roughly classified as either *non-dynamical* or *dynamical* meth-  
 208 ods. The class of non-dynamical methods only exploits geometrical properties of the data for  
 209 clustering, regardless of their temporal occurrence. The most used non-dynamical approach  
 210 is the k-means method, which clusters data points according to their minimal distance to ge-  
 211 ometrical centroids of point clouds<sup>20</sup>. Dynamical methods additionally take into account the  
 212 temporal changes of data, based on latent variables models such as hidden Markov models<sup>21</sup>.  
 213 This work considers a dynamical clustering method in which the existence of multiple states  
 214 is presumed, each having time-independent properties. Those states are presumed to have  
 215 a certain degree of persistence, and the system transitions between them during its evo-  
 216 lution. A simplified description of the dynamics is then given in terms of a set of locally  
 217 stationary linear vector autoregressive models (the cluster states). This method is coined  
 218 as FEM-BV-VAR approach (Finite Element clustering with bounded variation (FEM BV)  
 219 Vector autoregressive (VAR))<sup>16,17</sup>. Due to its proven utility in modeling transitional behav-  
 220 ior between persistent meta-stable states directly from data, FEM-BV-VAR has recently  
 221 become popular to study dynamical aspects of the atmosphere, ocean, and climate systems;  
 222 studies have tackled small-scale processes in the atmospheric boundary layer<sup>22,23</sup>, as well  
 223 as large-scale atmospheric and oceanic circulation<sup>13,24,25</sup>. Importantly, the method does not  
 224 rely on any underlying assumptions regarding the statistical stationarity of the data and,  
 225 hence, is applicable to problems where trends are present.

226 In the FEM-BV-VAR approach, a cluster is defined as a subset of the observed time  
 227 series of data whose evolution can be described approximately by a stationary linear vector  
 228 autoregressive model. The full time series is modeled as a set of such stationary VAR models,  
 229 with a switching process representing transitions between the cluster states. Since the states  
 230 are assumed to have a certain degree of persistence, the dynamical evolution of the system is  
 231 described by VAR models describing the fast-scale dynamics within a given state, while the  
 232 slow evolution is described by the switching process. Hence, the dynamics is decomposed  
 233 into two parts:

- 234 • a locally stationary fast auto-regressive (VAR) process,
- 235 • a slow hidden process that makes the system switch between different forms of such  
 236 auto-regressive processes (i.e. between the different states).

237 Within a given state, we assume the time evolution of the vector of observables  $\mathbf{x}_t$  to be  
 238 governed by

$$\mathbf{x}_t = \mu^{(i)} + \sum_{\tau=1}^m \mathbf{A}_\tau^{(i)} \mathbf{x}_{t-\tau} + \epsilon_t^{(i)} \quad (3)$$

where  $\mu^{(i)}$  is the mean of the  $i$ -th cluster,  $\mathbf{A}_\tau^{(i)}$  are matrices, and  $\epsilon_t^{(i)}$  is a white noise with a  
 covariance matrix  $\Sigma^{(i)}$ . A state of the system (or cluster)  $i$  is then characterized by its set  
 of parameters

$$\Theta_i = \left( \mu^{(i)}, \mathbf{A}_1^{(i)}, \dots, \mathbf{A}_m^{(i)}, \Sigma^{(i)} \right).$$

239 A set of  $K$  such models is assumed, with different model coefficients in (3), leading to  $K$   
 240 clusters. Determination of the optimal coefficients in (3) is done via minimization based on  
 241 the distance between the observations and the deterministic part of the model

$$g(\mathbf{x}_t, \theta(t)) = \left\| \mathbf{x}_t - \mu^{(i)}(t) - \sum_{\tau=1}^m \mathbf{A}_\tau^{(i)}(t) \mathbf{x}_{t-\tau} \right\|, \quad (4)$$

242 calculated for a fixed temporal realisation of parameters  $\theta(t)$ . The functional to minimize  
 243 also includes a cluster affiliation term that determines the set of model parameters the data  
 244 should be associated with and is then given as

$$L(\Theta, \Gamma(t)) = \sum_{t=0}^T \sum_{i=1}^K \gamma_i(t) g(\mathbf{x}_t, \Theta_i), \quad (5)$$

245 where  $\Theta$  denotes the collection of all  $\Theta_i$ , i.e.  $\Theta = (\Theta_1, \dots, \Theta_K)$  and  $T$  the time length of  
 246 the observed dynamics. The functions  $\Gamma(t) = (\gamma_1(t), \dots, \gamma_K(t))$  are the cluster affiliation

247 functions whose values give the probability of the data at time  $t$  to belong to cluster  $i$  and  
 248 should satisfy the following property at a given time  $t$

$$\sum_{i=1}^K \gamma_i = 1, \quad \gamma_i \geq 0 \quad \forall i = 1, \dots, K \quad (6)$$

249 The number  $K$  and the memory depth  $m$  are hyper-parameters that must be selected.  
 250 The assumption of local stationarity of the statistical process is finally enforced by setting a  
 251 persistence parameter  $C$ , which defines the maximum allowed number of transitions between  
 252 a total of  $K$  different statistical processes. This step regularises the minimization problem  
 253 by introducing the additional constraint on the total variation norm of the sequence

$$\sum_{t=0}^{T-1} |\gamma_i(t+1) - \gamma_i(t)| \leq C, \quad \forall i = 1, \dots, K. \quad (7)$$

254 This last hyper-parameter  $C$  is also more conveniently defined via the average persistence  $p$   
 255 as  $C = \frac{T}{p} - 1$ . The reader is referred to Horenko<sup>16</sup> and references therein for further details  
 256 about the method and the minimization process.

257 This method makes it possible to detect dynamical patterns that would not be detected  
 258 by a geometrical method such as the k-means: for instance, a change in frequency of the  
 259 signal or some oscillations with multiple amplitudes. It also provides a local linear model  
 260 for the data, on which the computation of the Covariant Lyapunov Vectors will be based.  
 261 However, it is important to bear in mind that three hyper-parameters ( $K, m, p$ ) have to be  
 262 selected when fitting a model.

## 263 B. Choosing the hyper-parameters

264 Statistical techniques based on information theory were developed to find the best hyper-  
 265 parameters of the FEM-BV-VAR (namely the number of clusters  $K$ , the memory depth  $m$   
 266 and the average persistence  $p$ )<sup>16,17</sup>. Here, physical understanding of the systems is also used  
 267 to choose  $K$  and  $m$ , as will be detailed when presenting the results. The persistence  $p$  is  
 268 selected via the so called L-curve method: as shown by Horenko<sup>16</sup>, the optimal value of  $p$  can  
 269 be determined as the edge point (or the point of maximal curvature) on a two- dimensional  
 270 plot, where one plots the total distance between the model and the data against the value  
 271 of  $p$ . In the application of the FEM-BV-VAR algorithm, the reconstructed signal has been  
 272 found to diverge in some configurations; hence, we have checked the output of the algorithm

273 manually and sometimes slightly modified  $p$  around its optimal value if the model, indeed,  
 274 diverges (results not shown).

### 275 C. Data-driven computation of the CLVs through the FEM-BV-VAR

276 The direct computation of CLVs requires an analytical expression of the linearized dy-  
 277 namics (in order to apply Froyland’s algorithms to the linear propagator). Hence, such a  
 278 computation is not feasible via purely data-driven approaches. The idea introduced by<sup>13</sup> is  
 279 to use the auto-regressive linear model obtained by the FEM-BV-VAR clustering step as an  
 280 underlying model to describe the dynamical system. Let us recall that the FEM-BV-VAR  
 281 gives us a VAR model for each of the  $K$  states

$$\mathbf{x}_t = \mu^{(i)}(t) + \sum_{\tau=1}^m \mathbf{A}_\tau^{(i)}(t) \mathbf{x}_{t-\tau} + \epsilon_t^{(i)}$$

From this we deduce a discrete linear dynamical system (here given for  $m = 3$ ) :

$$\begin{bmatrix} \mathbf{x}_{t+1} \\ \mathbf{x}_t \\ \mathbf{x}_{t-1} \end{bmatrix} = \begin{bmatrix} \mathbf{A}_1^{(i_{t+1})} & \mathbf{A}_2^{(i_{t+1})} & \mathbf{A}_3^{(i_{t+1})} \\ \mathbf{I} & \mathbf{0} & \mathbf{0} \\ \mathbf{0} & \mathbf{I} & \mathbf{0} \end{bmatrix} \begin{bmatrix} \mathbf{x}_t \\ \mathbf{x}_{t-1} \\ \mathbf{x}_{t-2} \end{bmatrix}$$

where  $i_{t+1}$  is the index of the state of the system at time  $t + 1$ . We can therefore compute the cocycle  $\mathcal{F}(t, t + \tau) = \mathcal{A}(t + \tau) \dots \mathcal{A}(t)$ , with

$$\mathcal{A}(t) = \begin{bmatrix} \mathbf{A}_1^{(i_{t+1})} & \mathbf{A}_2^{(i_{t+1})} & \mathbf{A}_3^{(i_{t+1})} \\ \mathbf{I} & \mathbf{0} & \mathbf{0} \\ \mathbf{0} & \mathbf{I} & \mathbf{0} \end{bmatrix}$$

282 Using the described approach, Quinn et al.<sup>13</sup> analyzed the dynamics of the North Atlantic  
 283 Oscillation, using daily means of the 500 hPa geopotential height as input data. The cluster-  
 284 ing framework was used to characterise the persistent states in the atmospheric circulation,  
 285 and the uncovered model was used to analyse the dynamical properties of different regimes.  
 286 In particular, a finite-time dimension measure for the linear dynamical system was used to  
 287 characterize the instability of each regime, thereby identifying the largest dimension to be  
 288 associated with a given state of the NAO, namely the blocked state. They also considered  
 289 the most unstable CLVs just before a transition from one state to another, to investigate

290 which atmospheric pattern was driving the instability. The results appeared consistent with  
291 previous studies based on different methodologies. This raised the following question: to  
292 what extent are the CLVs, computed in such a manner, significant dynamic indicators and  
293 can this method be applied to a large class of systems? In the following, we will test thor-  
294 oughly this method on systems for which many dynamical aspects are known: a fast-slow  
295 FitzHugh-Nagumo oscillator, a well-studied Von Kármán turbulent flow from a laboratory  
296 experiment, and a Lorenz 63 system.

#### 297 IV. OBSERVATIONS AND GUIDELINES

298 The purpose of the study is to determine the conditions under which the results obtained  
299 by computing the CLVs of a data series through the FEM-BV-VAR model are reliable. The  
300 method is applied to systems for which a priori knowledge of the states and of their stability  
301 exists. In terms of dynamical structure, the examples are introduced following an increase  
302 in complexity: the method is first applied on a fast-slow FitzHugh-Nagumo oscillator with  
303 two distinct time scales, then on data extracted from a laboratory experiment of a flow  
304 whose dynamics highlight a periodic orbit and a saddle point. Finally, the chaotic Lorenz  
305 attractor, which presents the most complex dynamics, is investigated.

306 Our main finding is that this procedure works well provided the studied system exhibits  
307 two properties (which are related to each other). Firstly, it should have a clear scale sepa-  
308 ration in time, that is, one should be able to distinguish a time scale gap between two (or  
309 more) phenomena in the dynamics, as, for instance, in standard fast-slow systems. Scale  
310 separation can be estimated in several different ways, depending on the availability of data  
311 and on the existence of differential equations to describe the dynamics<sup>26–29</sup>. Secondly, the  
312 system needs a (near-)neutral direction along trajectories which is invariant under the lin-  
313 ear(ized) dynamics: indeed, if the system does not have any neutral direction, the angle  
314  $\theta$  is no longer a relevant quantity to evaluate the stability of a state. This condition is  
315 frequently satisfied in physical systems, exhibiting invariant center manifolds where the hy-  
316 perbolic dynamics take place; these are exactly the *slow manifolds* in the fast-slow situation.  
317 For the data-driven approach to be successful, this neutral direction has to be preserved by  
318 the FEM-BV-VAR reconstructed model. This is a crucial challenge as we will see in the  
319 following.

320 **A. The case of a fast-slow FitzHugh-Nagumo oscillator**

As described in Section III A, the FEM-BV-VAR method is developed to study systems with a certain fast-slow structure, detecting the transition between states that are characterized by their respective fast dynamics. Therefore, the method is well-suited for models with time scale separation, expressed by a parameter  $0 < \epsilon \ll 1$ , that exhibit switches between different branches of the slow manifold consisting of equilibria of the fast subsystem. A by now canonical example of such a fast-slow system is the FitzHugh-Nagumo ODE (8) (see also Figure 2), which was derived as a simplification of the Hodgkin-Huxley model for an electric potential of a nerve axon<sup>30</sup>:

$$\begin{aligned}\epsilon \frac{dx}{d\tau} &= \epsilon \dot{x} = x - \frac{x^3}{3} - y, \\ \frac{dy}{d\tau} &= \dot{y} = x + a - by.\end{aligned}\tag{8}$$

Note that by a time change  $t = \tau/\epsilon$ , we may also write

$$\begin{aligned}\frac{dx}{dt} &= x' = x - \frac{x^3}{3} - y, \\ \frac{dy}{dt} &= y' = \epsilon(x + a - by).\end{aligned}\tag{9}$$

321 Setting  $\epsilon = 0$  in equation (9), one can study the *fast subsystem* for which  $y$  is a bifurcation  
 322 parameter and whose  $y$ -dependent set of equilibria is given by the curve  $y = x - x^3/3$ ,  
 323 also called *critical manifold*  $S_0$ . The cubic nonlinearity entails a bistable structure with  
 324 two fold points that mark a change of stability of the fast subsystem. Considering one of  
 325 the two (hyperbolically) stable branches of  $S_0$ , one may also take  $\epsilon = 0$  in equation (8)  
 326 and observe how the *slow subsystem* evolves along  $S_0$ . This gives a normal (or neutral)  
 327  $y$ -direction together with a hyperbolic  $x$ -direction, yielding, for  $\epsilon > 0$ , two branches of a  
 328 *slow manifold*  $S_\epsilon$  around the stable branches of  $S_0$  with the same stability properties<sup>31</sup>. At  
 329 the mentioned fold points this *normal hyperbolicity* breaks down and fast switches occur  
 330 between the two branches of the slow manifold (in accordance with the coloring in Figure 2  
 331 (a).) The described behavior is also called *relaxation-oscillation*, famously associated with  
 332 the van der Pol oscillator as a paradigm model, for which the FitzHugh-Nagumo ODE is a  
 333 slight generalization<sup>32</sup>. Summarizing, Figure 2 shows transitions between a left and a right  
 334 branch of a slow manifold. Along each of these branches, there is an actual neutral direction  
 335 complemented by a stable one for most of the time until both directions (almost) coincide  
 336 into a locally unstable direction around the fold (or transition) points. Hence, the alignment  
 337

338 variable  $\theta_{12}$ , where the stability of the CLVs is associated with the respective FTLEs, is an  
 339 appropriate observable for detecting such transitions, see also Figure 2 (b).

340 In Figure 2, the CLVs are computed via the FEM-BV-VAR clustering method: a FEM-  
 341 BV-VAR auto-regressive model is first fitted to the timeseries of observations  $(x, y)$  (see  
 342 Section III A), for which the best hyper-parameters are found to be  $K = 2$  (number of  
 343 clusters),  $m = 1$  (memory depth) and  $p = 175$  (persistence), with an integration step  
 344  $\tau = 0.003$ . In this example, the choice of  $K$ ,  $m$  and  $p$  is straightforward: the system has  
 345 two well identifiable states, leading to  $K = 2$ , and the averaged persistence can easily be  
 346 estimated by measuring the time spent by the system in each branch, leading to the estimate  
 347 for  $p$ . Then, the result is fairly robust to variations in  $m$ , such that the simplest value  $m = 1$   
 348 is selected for the analysis. Having obtained an explicit linear model purely from the time  
 349 series, the CLVs are approximated using the SVD-based algorithm (see Section II B), taking  
 350  $N = M = 10$  and  $n = 3$ . The CLV directions are robust under higher choices of  $N$ ,  $M$  and  
 351  $n$ . Note that the sign of the associated FTLEs depends on these choices; however, since  
 352 we are interested in manifesting the transition behavior happening on short time scales, the  
 353 small choices of  $N$ ,  $M$ ,  $n$  are suitable. The alignment  $\theta_{12}$  follows precisely the same profile

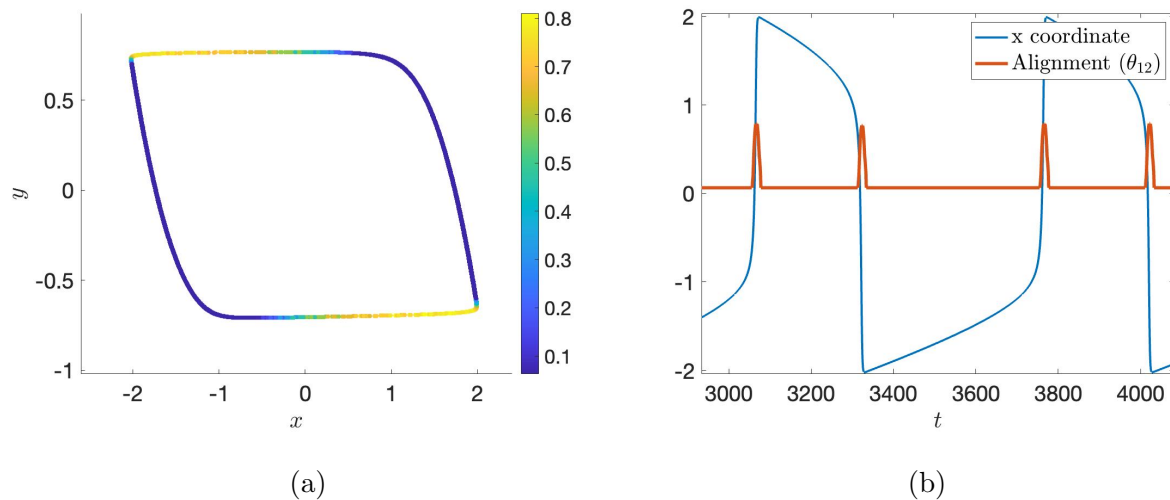


FIG. 2: (a) Trajectory in the  $x - y$  plane of the FitzHugh-Nagumo system, colored according to the alignment  $\theta_{12}$ , taking  $\epsilon = 0.01$ ,  $a = 0.4$ ,  $b = 0.3$  (standard choices, as in Sharafi et al.<sup>9</sup>). Yellow areas correspond to unstable CLVs being close to the neutral direction. (b) Time series of the  $x$  coordinate (blue) and of the alignment  $\theta_{12}$  (red).



354 as the one obtained through a direct computation of the CLVs from the linearization of the  
 355 explicit FitzHugh-Nagumo ODE (8). Sharafi et al.<sup>9</sup> also obtained a very similar pattern  
 356 when they studied the CLVs of the FitzHugh-Nagumo system, based on another algorithmic  
 357 procedure. Thus, the data-based method is successful for this example: via a pattern for  
 358  $\theta_{12}$ , one can clearly identify transitions between metastable states (corresponding with slow  
 359 manifolds) through the most (finite time) unstable CLV direction (corresponding with the  
 360 fast one).

361 The results confirm the hypothesis that systems with a clear time scale separation and  
 362 a slow manifold with an actual neutral mode are well-suited for using the FEM-BV-VAR  
 363 method on time series and then detecting transitions between branches of such a slow man-  
 364 ifold via the observable  $\theta_{12}$ .

## 365 B. The case of the von Kármán attractor

366 Next, the method is tested on a more complex example issued from laboratory turbulent  
 367 flows. In this case, the dynamics is indeed slightly more complex than in the FitzHug-  
 368 Nagumo model: as will be shown in this section, an attractor can be constructed for this  
 369 flow using an embedding procedure. This embedded attractor shows a periodic orbit as well  
 370 as a saddle point.

371 The experimental set-up is that of a von Kármán swirling flow, a device designed and  
 372 maintained at the Service de Physique de l'état Condensé of the Commissariat de l'Energie  
 373 Atomique in Saclay, France<sup>33-36</sup>. The von Kármán turbulent flow is generated in a vertical  
 374 cylinder filled with water and stirred by two coaxial, counter-rotating impellers. Those  
 375 impellers provide energy and momentum flux at the upper and lower ends of the cylinder  
 376 (see Fig. 2 in Dubrulle 2022<sup>36</sup>). We focus on the case where the impellers are driven by two  
 377 independent motors, operating in conditions such that the torques  $C_1$  and  $C_2$  applied by  
 378 the flow onto the top and bottom impellers are stationary. A control parameter is defined,  
 379 which is capable of tracking the symmetry of the forcing, namely  $\zeta = (C_1 - C_2)/(C_1 + C_2)$ .  
 380 To quantify the global response of the flow to the forcing, the rotating frequencies  $f_1$  and  $f_2$   
 381 of the two impellers are measured independently. This leads to the definition of the variable  
 382  $T = (f_1 - f_2)/(f_1 + f_2)$ , useful to characterize the symmetries of the flow. Indeed, previous  
 383 studies<sup>34,35</sup> have identified a precise relationship between values of  $T$  and instantaneous

384 configuration of the flow:  $T \simeq 0$  corresponds to a quasi-symmetric turbulent flow with two  
 385 large scale circulation cells close to the impellers, and turbulence concentrated around the  
 386 central section of the cylinder. For increasing  $|\zeta|$ , bifurcations of the flow are observed and  
 387 lead to positive or negative values of  $T$ . Those correspond to flow geometries where a single  
 388 large scale circulation structure occupies all the flow except for a turbulent boundary layer  
 389 located close to the upper or lower turbine, depending on the sign of  $T$ . When  $|\zeta| > 0.06$ ,  
 390 the von Kármán flow spontaneously switches among symmetric and bifurcated states and  
 391 the dynamical switches can be approximately described by a low-dimensional attractor<sup>35</sup>.

This attractor can be visualised with the embedding procedure, plotting  $(T_m, T_{m+\tau}, T_{m+2\tau})$ . Here we will consider the case  $\tau = 500$  and we refer to Faranda et al.<sup>35</sup> for further details on the experiment and the choice of the parameters. The obtained embedded attractor is represented in Fig.3. It shows two persistent states: on the left a meta-stable periodic orbit, and on the right a saddle point. The system spends more time spinning around the periodic orbit than around the saddle point. From the experimental data, one can only be hypothetical about the number of unstable directions of the saddle node; however, it is clear that this fixed point supports at least one stable (attracting) and at least one unstable (repulsive) direction. We apply the FEM-BV-VAR clustering method (see Section III A) to the time series of  $T$ . To that end, the first step is to choose the best FEM-BV-VAR hyper-parameters, namely the number of states  $K$ , the memory depth  $m$  and the persistence  $p$ . The embedding procedure highlights the existence of two clear states, a periodic orbit and a saddle node, thus  $K = 2$ . Then a grid search is performed to select values for  $m$  and  $p$ . As a criterion, we select the parameters that magnify the distinction between the periodic orbit and the saddle point, which corresponds to our intuition of the system behavior. The choice is based on a visual inspection of the output of the FEM-BV-VAR. The following values are finally selected:

$$k = 2, \quad m = 1, \quad p = 90.$$

392 The corresponding state affiliation is shown in Fig. 3, where each point of the embedded  
 393 attractor  $(T_m, T_{m+\tau}, T_{m+2\tau})$  is colored according to its affiliated FEM-BV-VAR cluster (also  
 394 called state). One sees that the yellow state clearly corresponds to the cycle, and the blue one  
 395 to the neighbourhood of the saddle point. The FEM-BV-VAR thus successfully captures the  
 396 dynamical states. Let us recall that beyond the state affiliation, the FEM-BV-VAR provides

397 a linear auto-regressive model to describe the local dynamics within a state.

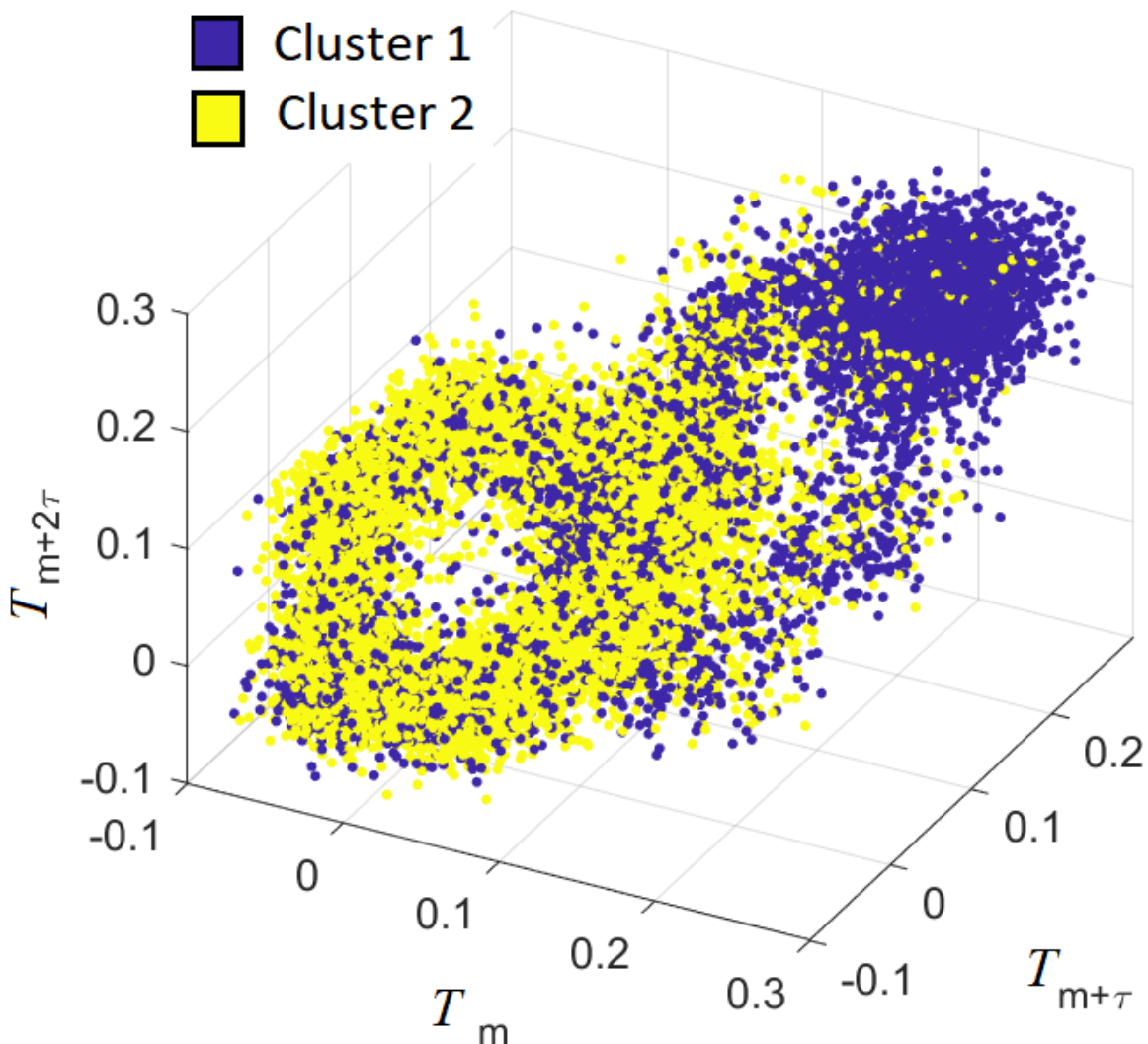


FIG. 3: FEM-BV-VAR clustering on the embedded attractor for the time series of the variable  $T$ , from the Von Kármán experimental data. Points that the algorithm detected as part of a neighbourhood of the periodic orbit are colored in yellow, and points that are associated to the saddle point, in blue. Parameters for the FEM-BV-VAR:  $K = 2$ ,  $m = 1$ ,  $p = 90$ .

398 The CLVs are then computed based on the linear model given by the FEM-BV-VAR.  
399 We do not expect to have an accurate computation of the CLVs in each point, but aim at  
400 estimating the relative stability of each state. Previous work<sup>35,36</sup> on the von Kármán flow  
401 experiment provide the results that can be expected: the periodic orbit is more strongly

402 stable than the saddle point, as it is associated with the symmetric flow (see Fig. 2 in  
 403 Faranda et al.<sup>35</sup>). We show that the data-driven approach to compute the CLVs can retrieve  
 404 this result directly from the data, looking at the alignment  $\theta_{12}$  between the most unstable  
 405 CLV and the near-neutral one.

406 To that end, Froyland’s algorithm (see Section II B) is applied to the linear auto-regressive  
 407 model given by the FEM-BV-VAR clustering. Three parameters need to be selected to apply  
 408 the algorithm: the number of push forward steps  $M$ , the number of backward steps  $N$  and  
 409 the correction step  $n$ . For simplicity we take  $N = M$ . A grid search is then applied on  
 410  $N(= M)$  and  $n$ . For each configuration, the CLVs and the alignment  $\theta_{12}$  (as defined in  
 411 Eq. (2)) are computed. Fig. 4 shows the obtained result for one configuration of  $N(= M)$   
 412 and  $n$ , which is consistent with the expected result. The color corresponds to the value of  
 413 the alignment  $\theta_{12}$ , plotted on the embedded attractor, for  $N = M = 30$  and  $n = 1$ . Around  
 414 the periodic orbit the values of  $\theta_{12}$  are clearly lower than around the saddle point, which  
 415 means that the orbit is more strongly stable. However, the grid search (Fig. 5) shows that  
 416 the result is not completely robust and depends on the choice of  $N$  and  $n$ .

417 To highlight the relative stability of the periodic orbit compared to the saddle point, the  
 418 following difference is defined:

$$\Delta_{VKM} = \text{average of } \theta_{12} \text{ around the periodic orbit} - \text{average of } \theta_{12} \text{ around the saddle point} \quad (10)$$

419 Fig. 5 shows, for each choice of  $(N, n)$ , the value of the difference  $\Delta$  between the average  
 420 alignment  $\theta_{12}$  on the orbit and around the saddle point. In most configurations, the difference  
 421 is negative, that is to say the periodic orbit is more strongly stable than the saddle point  
 422 (which is the expected result). However, care is needed because for some choices of  $(N, n)$   
 423 the result is precisely the opposite. Thus,  $N$  and  $n$  should be large enough, but for larger  
 424 values of  $N$ ,  $\theta_{12}$  appears to become noisy (likely due to accumulation of numerical errors).  
 425 Therefore the choice of  $N$  and  $n$  is a sensitive step, for which no systematic guidelines  
 426 are available. However, the grid search used in this study supports a suitable selection of  
 427 parameters, in combination with some a priori knowledge of the dynamics.

428 Nonetheless, this shows that for well suited values of the FEM-BV-VAR parameters (the  
 429 number of states  $K$ , the memory depth  $m$  and the persistence  $p$ ) and of Froyland’s algorithm  
 430 parameters  $N$  and  $n$ , one can obtain a very insightful information on the relative stability

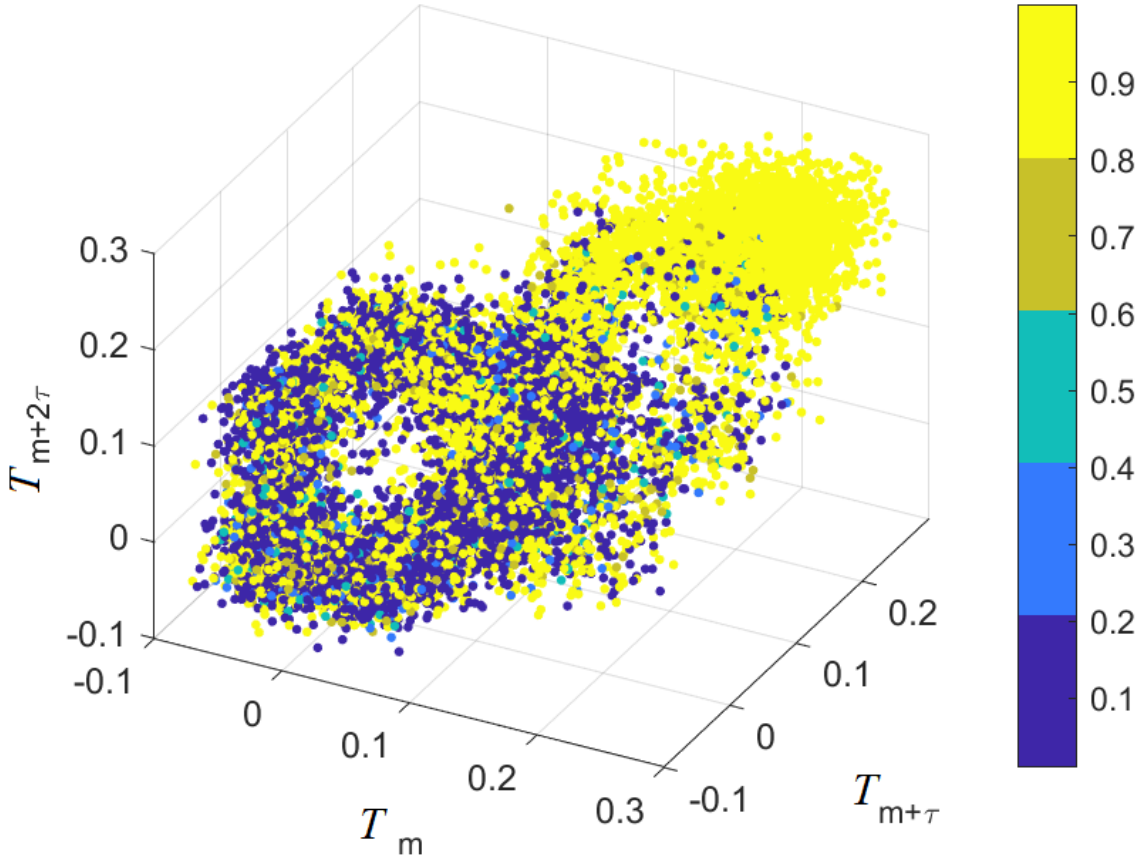


FIG. 4: CLVs alignment  $\theta_{12}$  on the VKM embedded attractor. Colors correspond to the value of  $\theta_{12}$ . In this configuration, the periodic orbit (in blue) appears to be more strongly stable than the saddle point (in yellow), which is the expected result. Parameters for the FEM-BV-VAR:  $K = 2$ ,  $m = 1$ ,  $p = 80$ . Parameters for Froyland's algorithm:  $N = 30$ ,  $n = 1$

431 of the states of the system, without any *a priori* information other than the raw data. This  
 432 illustrates the potential validity of this method, even with experimental data. The example  
 433 also supports our hypothesis that the existence of both a scale separation and a neutral  
 434 direction is essential for the success of this method. In the von Kármán flow embedded  
 435 attractor, one clearly has a scale separation in the sense that the trajectory oscillates for  
 436 some time around one state (either the cycle or the point), and then quickly switches to  
 437 the other state, with a characteristic time much faster than the oscillation. The existence  
 438 of a neutral direction is more delicate to conclude, given that we do not have an underlying

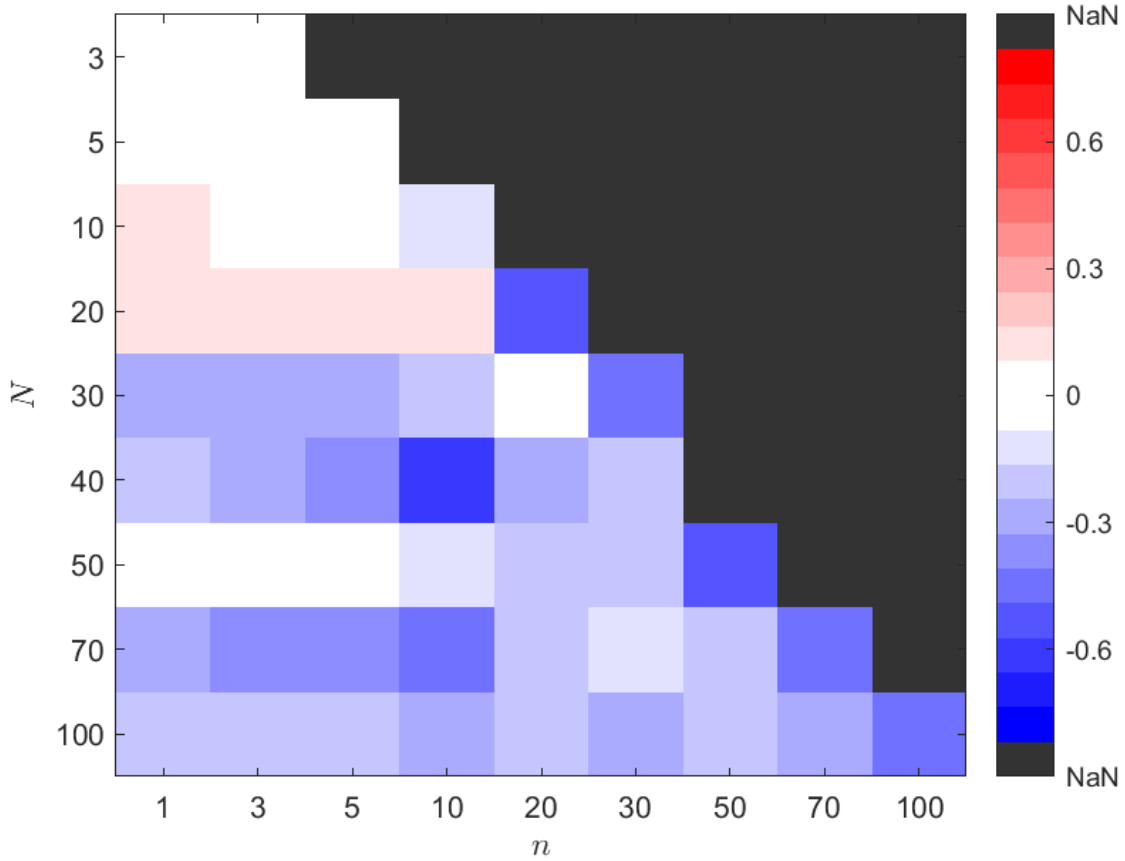


FIG. 5: Difference  $\Delta_{VKM}$  between the average alignment in state 1 (periodic orbit) and 2 (saddle point), as defined in Eq. (10).  $N$  is the number of backward and forward steps (note that  $M = N$ ), and  $n$  is the correction step (see II B). The blue areas correspond to the set of parameters for which the cycle is more strongly stable than the saddle point, which is expected.

439 analytical model. However, the existence of the anticipated neutral direction is consistent  
 440 with the observed quasi-periodic motion.

### 441 C. On a Lorenz 63 model

442 To complete the study, the method is tested on a single Lorenz 63 system, with the usual  
 443 parameters for obtaining a chaotic attractor ( $\sigma = 10, \beta = 8/3, \rho = 28$ )<sup>37</sup> :

$$\begin{aligned}
\frac{dx}{dt} &= \sigma(y - x), \\
\frac{dy}{dt} &= x(\rho - z) - y, \\
\frac{dz}{dt} &= xy - \beta z.
\end{aligned}
\tag{11}$$

The attractor is self-excited with respect to three equilibria: two unstable equilibria at the center of each wing and one saddle node at the origin, see Fig. 6. The system exhibits no attracting limit cycle such that the oscillations within each wing are aperiodic, exhibiting no asymptotically exact neutral direction for the linearization. The dynamics in each of the wings is sometimes described as metastable, with fast switches between them, such that one might think of a time scale separation. However, the associated patterns are highly irregular and not clearly associated to fast-slow dynamics (see also Figure 7). Dynamically speaking, this system is the most complex of this study. Regarding the Lyapunov exponents, a computation from the set of equations (11) gives (as computed through Ginelli’s procedure<sup>4</sup>):

$$\lambda_1 = 0.9, \lambda_2 = 0.005, \lambda_3 = -14.5.$$

444 These correspond to an unstable, a near-neutral and a stable direction respectively. Using  
445 the Froyland algorithm, one can compute the CLVs along the trajectory using the analytical  
446 expression of the equations (see Section II B). Fig. 6 shows the value of the alignment  $\theta_{12}$   
447 (cosine of the angle between the most unstable CLV and the near-neutral one), plotted  
448 onto the trajectory of the Lorenz 63 system. Blue areas correspond to low values of  $\theta_{12}$ ,  
449 therefore to more stable regions, and yellow areas to more unstable accordingly. Previous  
450 studies showed that the alignment of CLVs computed directly from the set of equations was  
451 a relevant tool to predict regime transition in the Lorenz 63 model<sup>11</sup>. In this study, we aim  
452 at assessing whether the FEM-BV-VAR model captures enough dynamical information for  
453 the approximated data-driven CLVs to follow a similar pattern as in Fig. 6.

As for the previous examples, one has first to choose the three parameters of the FEM-BV-VAR (namely the number of states  $K$ , the memory depth  $m$  and the persistence  $p$ , see Section III A), which is harder in this example.  $K = 2$  comes naturally as the attractor has two wings. As explained in Section III B, the value of the persistence  $p$  can be optimally chosen thanks to the L-curve method, provided we already fixed  $K$  and  $m$ . To choose  $m$ ,

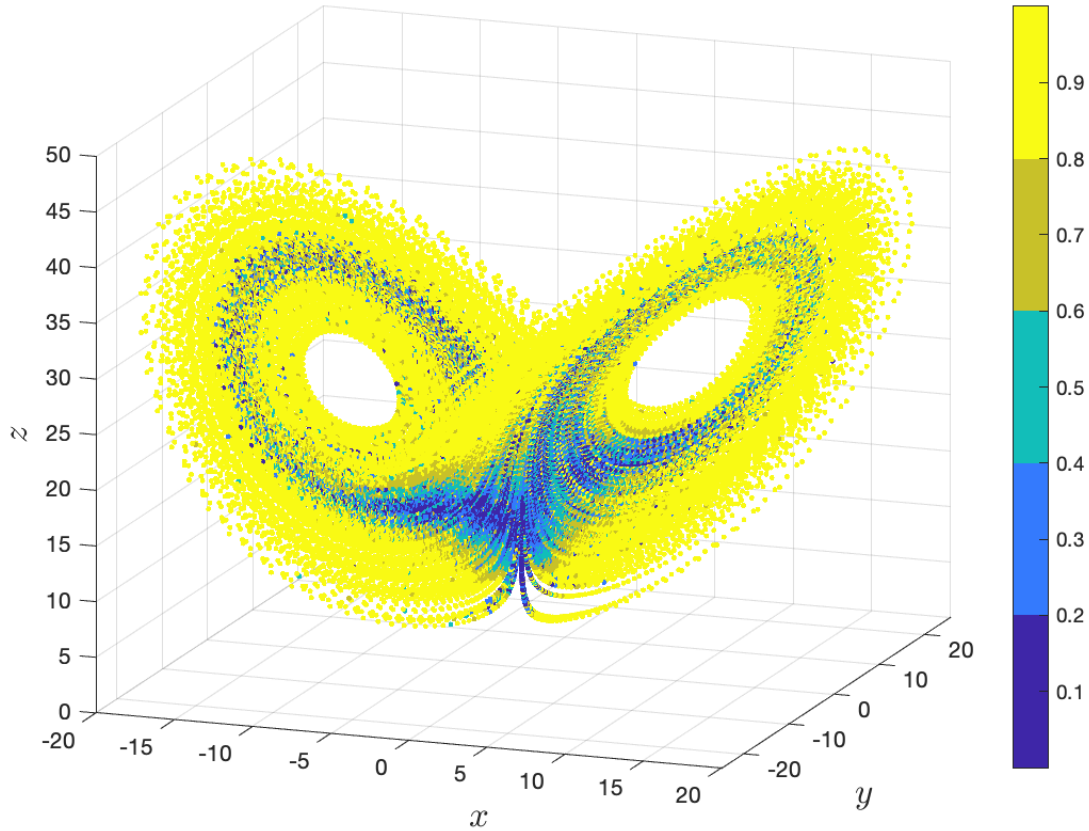


FIG. 6: Froyland’s algorithm on a simple Lorenz 63,  $N = 100$ ,  $\tau = 0.01$  (integration step).

The colors show the alignment  $\theta_{12}$ , as defined in Eq. 2. Blue areas correspond to more stable areas, where the most unstable CLV and the near-neutral one are close to being orthogonal. Conversely, yellow areas are very unstable. This result proves robust under an increase of  $N$ , provided  $N \geq 50$ .

the method is tested with different values of  $m$  ranging from 1 to 5. For  $m \leq 2$ , the CLVs algorithm does not converge well on the FEM-BV-VAR reconstructed model. Thus we take  $m = 3$ , the smallest value for which the convergence is good enough. The higher  $m$ , the more complex the model can be (since the dimension of the auto-regressive model is  $dim \times m$ ). With  $m \leq 2$ , the model may be too simple and may not capture the oscillatory patterns of the original system. Hence, the final choice is

$$K = 2, m = 3, p = 29,$$

454 where  $p$  is chosen thanks to the L-curve method. Fig. 7 shows an extract of the time series



455 of the original data (in yellow), the reconstructed model (in red) and the states affiliation  
 456 found by the FEM-BV-VAR clustering (background in blue). Note that the neutral direction  
 457 almost exists in the Lorenz system and leads to the oscillating dynamics. However, the FEM-  
 458 BV-VAR reconstruction in Fig. 7 shows that the oscillations within a state are lost. This is a  
 459 sign that the fitted AR model loses the near-neutral direction: an insight that is important  
 460 for the following CLV analysis.

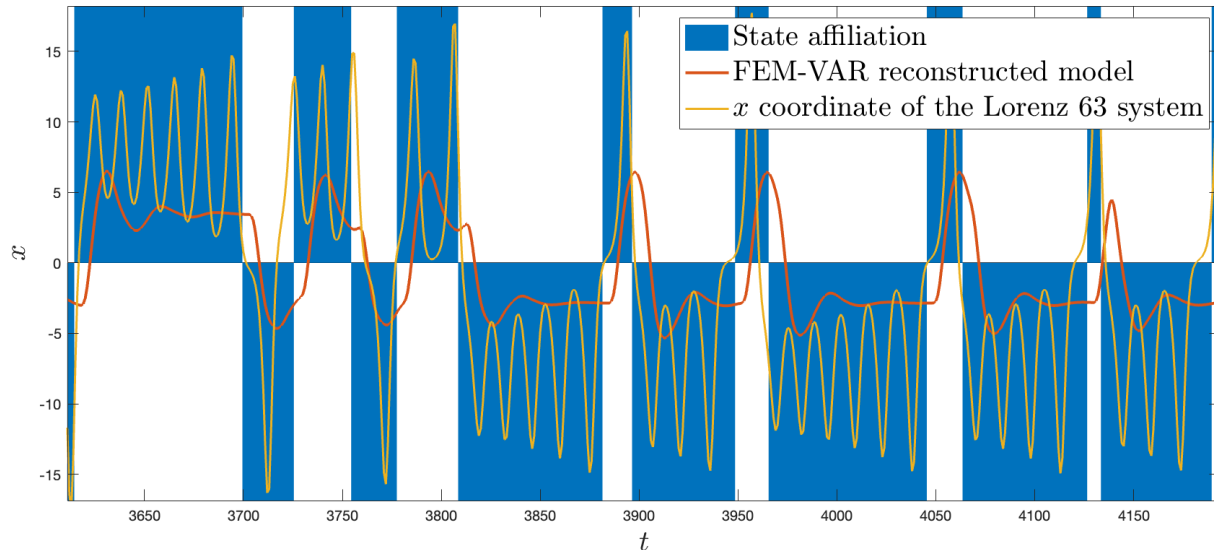


FIG. 7: FEM-BV-VAR clustering applied to a Lorenz 63. First component of the Lorenz  
 system (yellow), states affiliation (blue and white strips) and reconstruction by the  
 FEM-BV-VAR (red). For  $K = 2$ ,  $m = 3$ ,  $p = 29$ .

461 The next step is to choose  $N = M$  (the number of push backward and push forward  
 462 steps) and  $n$  (the correction steps) to run the CLVs algorithms (see Section II B). It turns  
 463 out that the obtained result depends highly on this choice, as for the Von Kármán flow data,  
 464 except that for the Lorenz system the range of validity of the method is much narrower.  
 465 For intermediate values, such as  $N = 10$  and  $n = 5$ , one can get some information on the  
 466 attractor thanks to the alignment  $\theta_{12}$  obtained through the FEM-BV-VAR approach. Fig. 8  
 467 provides a picture that can be compared with the expected result from Fig. 6. The absolute  
 468 values of  $\theta_{12}$  along the trajectories are not the same as expected. However, one can see that  
 469 the outbound of the wings is found to be less stable than the bulk. Hence, the method  
 470 provides again an insight on the dynamics which is, however, less precise and accurate than  
 471 in the two previous examples.

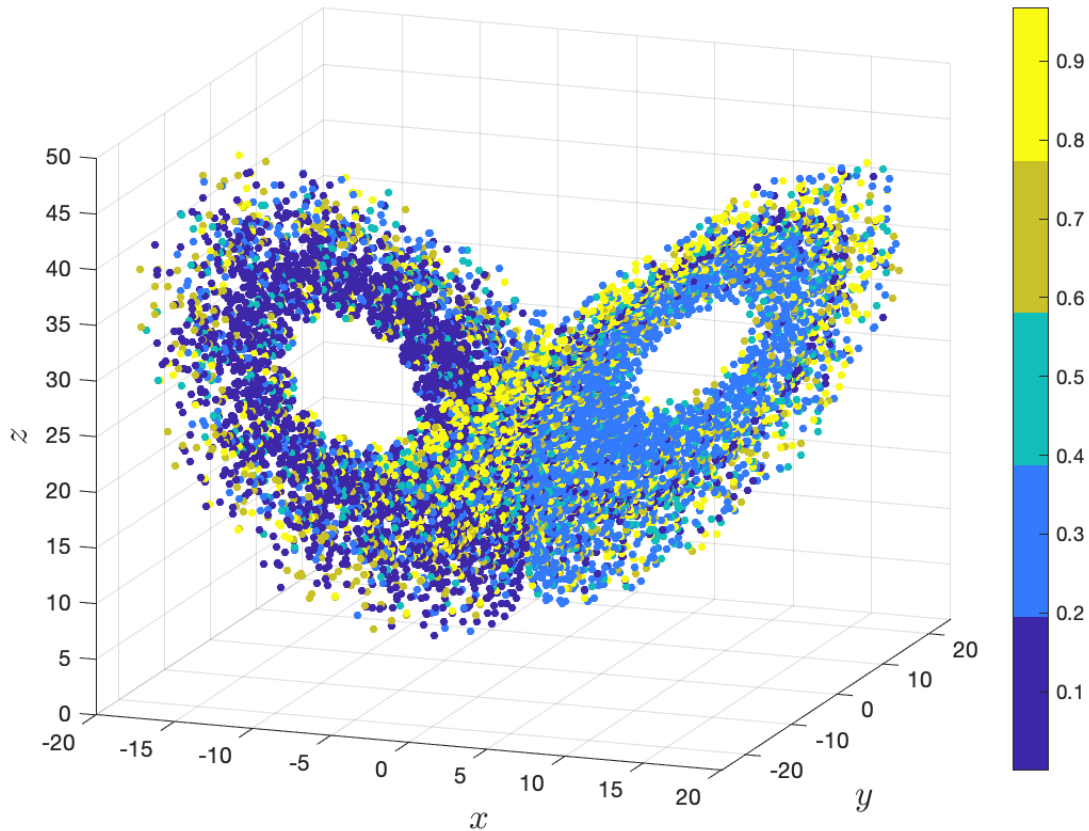


FIG. 8: Alignment of CLVs on a Lorenz 63 system, obtained thanks to the FEM-BV-VAR model. In color:  $\theta_{12}$ . One can see that the outbound of the wings is found to be less stable than the bulk. CLVs computed with the Froyland algorithm ( $N = 10$ ,  $n = 5$ ), from the FEM-BV-VAR reconstruction with  $K = 2$ ,  $m = 3$ ,  $p = 29$ .

472 To evaluate the range of validity of the method, the same picture is generated for  $N$   
 473 ranging from 3 to 100 and  $n$  from 1 to 100. Two criteria are used to assess the relevance of  
 474 the obtained result. First, given that the distribution of the value  $\theta_{12}$  has to be the same in  
 475 each wing (the two wings are dynamically symmetric), the average of  $\theta_{12}$  is expected to be  
 476 the same in each wing. To monitor that, one can look at the difference between the average  
 477 value of  $\theta_{12}$  over the two wings:

$$\Delta_{Lorenz} = \text{average of } \theta_{12} \text{ over the left wing} - \text{average of } \theta_{12} \text{ over the right wing} \quad (12)$$

478 Secondly, to have an indicator of noisiness of the obtained time series for  $\theta_{12}$ , one can look  
 479 at the total variation

$$TV = \sum_i |\theta_{12}(i+1) - \theta_{12}(i)| \quad (13)$$

480 The previously shown Fig. 8 was chosen to be the configuration that minimizes the total  
 481 variation, keeping it strictly positive.

482 Fig. 9 shows, for each choice of  $(N, n)$ , the value of the difference  $\Delta_{Lorenz}$  between the  
 483 average alignment  $\theta_{12}$  over the left wing and over the right one. This value is expected to be  
 484 as close as possible to zero. One can see that for small values of  $N$  and  $n$ , the output is very  
 485 asymmetric (blue zone in the bottom left), as well as for large values of  $N$  (red strip on the  
 486 top). As previously explained, such an asymmetry is not physically relevant. Moreover, the  
 487 total variation (Eq. (13)) tends to increase as  $N$  and  $n$  increase. Thus, unlike for the von  
 488 Kármán flow data, the range of validity of this method in the  $N$ - $n$  plane is small, making  
 489 this method hardly usable in practice for the Lorenz system. While one can have some  
 490 systematic methods to tune the FEM-BV-VAR parameters ( $K$ ,  $m$  and  $p$ , see Section III B),  
 491 no such tools exist to choose  $N$  and  $n$ .

492 This observation supports our key finding: the procedure does not work well when the  
 493 system has no clear time-scale separation and when the FEM-BV-VAR reconstruction does  
 494 not preserve the existence of an invariant neutral direction. As mentioned above, one can  
 495 see in Figure 7 that the FEM-BV-VAR reconstructed model (in red) does not exhibit the  
 496 oscillations within the wings that are characteristic of the original model (in yellow). Yet,  
 497 those oscillations are important to capture the dynamics and predict the transition from  
 498 one wing to the other, as suggested by Lorenz in his original paper<sup>37</sup>. In fact, the FEM-BV-  
 499 VAR model seems not be able to preserve the existence of a neutral direction (of which the  
 500 oscillatory dynamics are a characteristic feature). Figure 10 shows the alignment  $\theta$  (that  
 501 is to say the cosine of the angle) between the tangent to the trajectory and the expected  
 502 near-neutral CLV (as there are only three dimensions, the near-neutral CLV is the second  
 503 one in this case). On the left, this alignment is computed for the Lorenz 63 system directly  
 504 from the analytical expression. One clearly sees that almost everywhere the second CLV  
 505 and the flow are aligned, which confirms the existence of a neutral direction in this system.  
 506 However, the same computation but with the CLVs computed through the FEM-BV-VAR  
 507 model shows different results. The picture is completely erratic, which means that the  
 508 neutral direction is (almost) entirely lost. In summary the FEM-BV-VAR model fails to

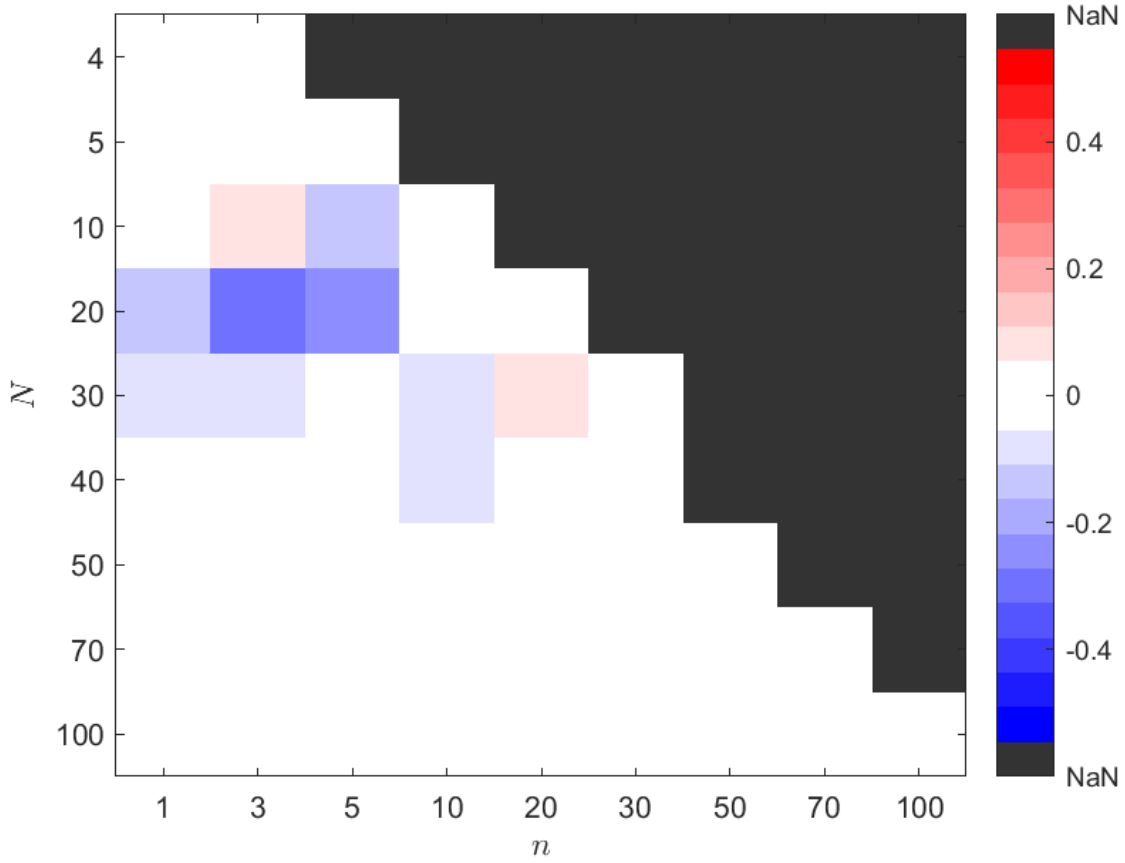


FIG. 9: Pcolor plot of  $\Delta_{Lorenz}$ , the difference between the average value of  $\theta_{12}$  over the two wings (see Eq. 12).  $N$  is in ordinate and  $n$  in abscissa. As the two wings are symmetric, in theory this difference should be close to zero (white area). One can see that for  $N$  and  $n$  not large enough,  $\Delta_{Lorenz}$  can be far from zero, which means that the method does not converge well with this values.

509 capture the irregular oscillations of the system within each wing associated with such near-  
 510 neutral directions. This is most likely related to the simple, linear model structure assumed  
 511 in the FEM-BV-VAR approach.

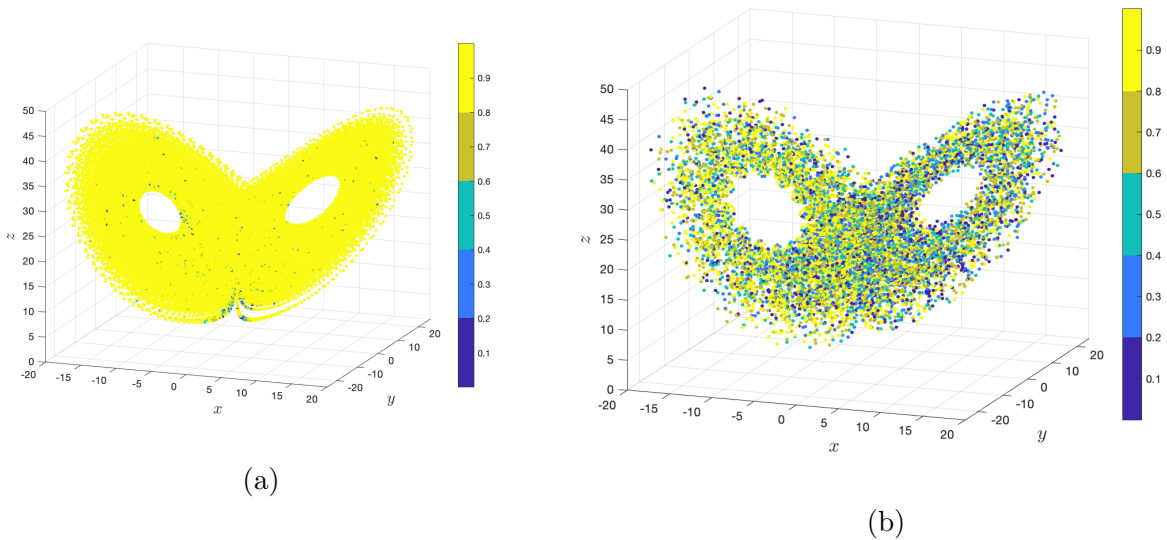


FIG. 10: (a) Alignment  $\theta$  between the flow (tangent to the trajectory in each point) and the near neutral CLV, directly computed on a Lorenz system. Yellow corresponds to closely aligned vectors. (b) Same angle, but this time with the near neutral CLV computed on the FEM-BV-VAR reconstructed model. One can clearly see that in the first case, the near neutral CLV does correspond to the direction of the flow. However with the FEM-BV-VAR reconstruction, one completely loses this alignment.

512 **V. CONCLUSION**

513 The method described in this paper and suggested in earlier work by Quinn et al.<sup>13</sup> makes  
 514 it possible to compute an approximation of the Covariant Lyapunov Vectors (CLVs) from  
 515 data series. It is based on the FEM-BV-VAR clustering scheme, which provides piece-wise  
 516 auto-regressive linear models for the data. This model being built, one can compute an  
 517 approximation of the CLVs. Under some conditions, the procedure seems to capture enough  
 518 information on the dynamics to be able to give us the relative stability of the different areas  
 519 of the phase space (that is to say, in this framework, the stability of the trajectory within  
 520 each of the FEM-BV-VAR cluster). Information about stability of the trajectory is given  
 521 by the analysis of the alignment between the most unstable (finite time) Lyapunov vector  
 522 and the nearly neutral one (denoted  $\theta_{12}$ ).

523 We claim that this procedure works well provided the studied system exhibits two prop-

524 erties. First, it should have a clear scale separation in time, that is to say one should be able  
525 to distinguish a temporal scale gap between two (or more) phenomena in the dynamics, as,  
526 for instance, in standard fast-slow systems.

527 Secondly, the system has to support a dynamically invariant neutral direction in its  
528 linearization and, importantly, this neutral direction has to be preserved as much as possible  
529 by the FEM-BV-VAR reconstructed model. To support this hypothesis, we have tested the  
530 validity of the method on three different systems with an increasing dynamical complexity:  
531 the fast-slow FitzHugh-Nagumo oscillator, an embedded attractor built from von Kármán  
532 flow data that exhibits a periodic orbit along with an saddle point, and finally a classic  
533 Lorenz 63 chaotic attractor.

534 In the case of the FitzHugh-Nagumo oscillator, the method yields good performances: one  
535 can find transitions precisely via the pattern of  $\theta_{12}$ , as the method clearly identifies switches  
536 between slow metastable regimes via unstable fast dynamics. This system exhibits a clear  
537 time-scale separation that makes it possible for the FEM-BV-VAR model to capture most  
538 of the relevant dynamical information, and especially to preserve the neutral direction. The  
539 case of the von Kármán flow shows that the method can be relevant even with experimental  
540 data, provided the dynamics exhibits a clear scale separation that allows the FEM-BV-VAR  
541 to preserve the existence of a neutral direction in the reconstructed model. It also indicates  
542 that one should be careful when tuning the values of  $N$ ,  $M$  and  $n$ : they must be large  
543 enough for Froyland’s algorithm to converge, but not too large to avoid the accumulation of  
544 numerical errors. Finally, the Lorenz 63 example shows that for a system without a clear time  
545 scale separation, the results are highly dependent on the hyper-parameters and therefore the  
546 method is prone to fail. Due to its simple, linear model structure, the FEM-BV-VAR cannot  
547 capture irregular, complicated short term dynamical patterns (as the oscillation around the  
548 wing centers), and the reconstructed model does not show any direction that can be seen as  
549 (near-)neutral.

550 Note that, while the reference approach by Quinn et al.<sup>13</sup> assumes VAR models within  
551 clusters, the clustering framework introduced by Horenko<sup>16</sup> is general and can accommodate  
552 more flexible model structures. Some alternative examples using different model structures  
553 can be found in Metzner et al.<sup>17</sup> and in de Wiljes et al.<sup>38</sup>. In particular, Boyko et al.<sup>39</sup>  
554 recently extended this model-based clustering approach to enable the use of continuous  
555 models, effectively fitting a nonstationary, nonlinear stochastic differential equation (SDE)

556 to timeseries of observations. Hence the data-driven computations of the CLVs could be  
557 extended to using such a SDE-based clustering for the required model fitting step. Such  
558 a future extension, based on a likely more faithful representation of complex multiscale  
559 dynamics, may lead to more accurate estimation of the CLVs and hence to a better approach  
560 to study transitions in complex systems such as the climate system.

## 561 ACKNOWLEDGMENTS

562 The authors thank the Ecole Normale Supérieure (ENS) for financial support enabling a  
563 research exchange of AV during which this work was started. The authors acknowledge B  
564 Dubrulle, F Daviaud and B Saint-Michel for granting the use of the von Kármán data. The  
565 work benefited from discussions with Peter Koltai. M.E. has been supported by Germany’s  
566 Excellence Strategy – The Berlin Mathematics Research Center MATH+ (EXC-2046/1,  
567 project ID: 390685689).

## 568 DATA AVAILABILITY

569 The data that support the findings of this study are available from the corresponding  
570 author upon reasonable request.

## 571 REFERENCES

- 572 <sup>1</sup>A. Katok and B. Hasselblatt, *Introduction to the modern theory of dynamical systems*, 54  
573 (Cambridge university press, 1997).
- 574 <sup>2</sup>P. Manneville, *Instabilities, chaos and turbulence*, Vol. 1 (World Scientific, 2010).
- 575 <sup>3</sup>D. Ruelle, “Sensitive dependence on initial condition and turbulent behavior of dynamical  
576 systems,” *Annals of the New York Academy of Sciences* **316**, 408–416 (1979).
- 577 <sup>4</sup>F. Ginelli, P. Poggi, A. Turchi, H. Chaté, R. Livi, and A. Politi, “Characterizing dynamics  
578 with covariant lyapunov vectors,” *Physical review letters* **99**, 130601 (2007).
- 579 <sup>5</sup>C. L. Wolfe and R. M. Samelson, “An efficient method for recovering lyapunov vectors  
580 from singular vectors,” *Tellus A: Dynamic Meteorology and Oceanography* **59**, 355–366  
581 (2007).

- 582 <sup>6</sup>S. Gilmore, “Lyapunov exponents and temperature transitions in a warming australia,”  
583 *Journal of Climate* **32**, 2969 – 2989 (2019).
- 584 <sup>7</sup>F. Nazarimehr, S. Jafari, S. M. R. H. Golpayegani, and J. Sprott, “Can lyapunov expo-  
585 nent predict critical transitions in biological systems?” *Nonlinear Dynamics* **88**, 1493–1500  
586 (2017).
- 587 <sup>8</sup>Z. Toth and E. Kalnay, “Ensemble forecasting at nmc: The generation of perturbations,”  
588 *Bulletin of the american meteorological society* **74**, 2317–2330 (1993).
- 589 <sup>9</sup>N. Sharafi, M. Timme, and S. Hallerberg, “Critical transitions and perturbation growth  
590 directions,” *Physical Review E* **96**, 032220 (2017).
- 591 <sup>10</sup>M. W. Beims and J. A. Gallas, “Alignment of lyapunov vectors: A quantitative criterion  
592 to predict catastrophes?” *Scientific reports* **6**, 1–7 (2016).
- 593 <sup>11</sup>E. L. Brugnago, J. A. C. Gallas, and M. W. Beims, “Predicting regime changes and  
594 durations in lorenz’s atmospheric convection model,” *Chaos: An Interdisciplinary Journal*  
595 *of Nonlinear Science* **30**, 103109 (2020), <https://doi.org/10.1063/5.0013253>.
- 596 <sup>12</sup>C. Quinn, T. J. O’Kane, and V. Kitsios, “Application of a local attractor dimension to  
597 reduced space strongly coupled data assimilation for chaotic multiscale systems,” *Nonlinear*  
598 *Processes in Geophysics* **27**, 51–74 (2020).
- 599 <sup>13</sup>C. Quinn, D. Harries, and T. J. O. Kane, “Dynamical analysis of a reduced model for the  
600 north atlantic oscillation,” *Journal of the Atmospheric Sciences* **78**, 1647 – 1671 (2021).
- 601 <sup>14</sup>G. Froyland, T. Hüls, G. P. Morriss, and T. M. Watson, “Computing covariant Lyapunov  
602 vectors, Oseledets vectors, and dichotomy projectors: a comparative numerical study,”  
603 *Phys. D* **247**, 18–39 (2013).
- 604 <sup>15</sup>C. Martin, N. Sharafi, and S. Hallerberg, “Estimating covariant lyapunov vectors from  
605 data,” *Chaos: An Interdisciplinary Journal of Nonlinear Science* **32**, 033105 (2022).
- 606 <sup>16</sup>I. Horenko, “On the identification of nonstationary factor models and their application to  
607 atmospheric data analysis,” *Journal of the Atmospheric Sciences* **67**, 1559–1574 (2010).
- 608 <sup>17</sup>P. Metzner, L. Putzig, and I. Horenko, “Analysis of persistent nonstationary time series  
609 and applications,” *Communications in Applied Mathematics and Computational Science*  
610 **7**, 175–229 (2012).
- 611 <sup>18</sup>V. I. Oseledec, “A multiplicative ergodic theorem. Characteristic Ljapunov, exponents of  
612 dynamical systems,” *Trudy Moskov. Mat. Obšč.* **19**, 179–210 (1968).



- 613 <sup>19</sup>B. Deremble, F. D’Andrea, and M. Ghil, “Fixed points, stable manifolds, weather regimes,  
614 and their predictability,” *Chaos: An Interdisciplinary Journal of Nonlinear Science* **19**,  
615 043109 (2009).
- 616 <sup>20</sup>J. A. Hartigan and M. A. Wong, “Algorithm AS 136: A K-Means Clustering Algorithm,”  
617 *Journal of the Royal Statistical Society. Series C (Applied Statistics)* **28**, 100–108 (1979),  
618 publisher: [Wiley, Royal Statistical Society].
- 619 <sup>21</sup>L. Rabiner, English “A Tutorial on Hidden Markov-Models and Selected Applications in  
620 Speech Recognition,” *Proceedings of the Ieee* **77**, 257–286 (1989).
- 621 <sup>22</sup>N. Vercauteren and R. Klein, “A Clustering Method to Characterize Intermittent Bursts of  
622 Turbulence and Interaction with Submesoscale Motions in the Stable Boundary Layer,” *Journal*  
623 *of Atmospheric Sciences* **72**, 1504–1517 (2015).
- 624 <sup>23</sup>V. Boyko and N. Vercauteren, “Multiscale Shear Forcing of Turbulence in the Nocturnal  
625 Boundary Layer: A Statistical Analysis,” *Boundary-Layer Meteorology* **179**, 43–72 (2021),  
626 publisher: Springer Netherlands.
- 627 <sup>24</sup>T. J. O’Kane, J. S. Risbey, C. Franzke, I. Horenko, and D. P. Monselesan, “Changes  
628 in the metastability of the midlatitude southern hemisphere circulation and the utility of  
629 nonstationary cluster analysis and split-flow blocking indices as diagnostic tools,” *Journal*  
630 *of the atmospheric sciences* **70**, 824–842 (2013).
- 631 <sup>25</sup>T. J. O’Kane, R. J. Matear, M. A. Chamberlain, J. S. Risbey, B. M. Sloyan, and  
632 I. Horenko, en “Decadal variability in an OGCM Southern Ocean: Intrinsic modes, forced  
633 modes and metastable states,” *Ocean Modelling* **69**, 1–21 (2013).
- 634 <sup>26</sup>C. Rödenbeck, C. Beck, and H. Kantz, “Dynamical systems with time scale separation:  
635 averaging, stochastic modelling, and central limit theorems,” in *Stochastic Climate Models*  
636 (Springer, 2001) pp. 189–209.
- 637 <sup>27</sup>J. Wouters and V. Lucarini, “Multi-level dynamical systems: Connecting the ruelle re-  
638 sponse theory and the mori-zwanzig approach,” *Journal of Statistical Physics* **151**, 850–860  
639 (2013).
- 640 <sup>28</sup>S. Shoffner and S. Schnell, “Approaches for the estimation of timescales in nonlinear dy-  
641 namical systems: Timescale separation in enzyme kinetics as a case study,” *Mathematical*  
642 *biosciences* **287**, 122–129 (2017).
- 643 <sup>29</sup>T. Alberti, D. Faranda, R. V. Donner, T. Caby, V. Carbone, G. Consolini, B. Dubrulle,  
644 and S. Vaienti, “Small-scale induced large-scale transitions in solar wind magnetic field,”

645 The Astrophysical journal letters **914**, L6 (2021).

646 <sup>30</sup>R. FitzHugh, “Mathematical models of threshold phenomena in the nerve membrane,”  
647 Bull. Math. Biophysics **17** (1955).

648 <sup>31</sup>N. Fenichel, “Geometric singular perturbation theory for ordinary differential equations,”  
649 J. Differential Equations **31**, 53–98 (1979).

650 <sup>32</sup>C. Kuehn, *Multiple time scale dynamics*, Applied Mathematical Sciences, Vol. 191  
651 (Springer, Cham, 2015) pp. xiv+814.

652 <sup>33</sup>P.-P. Cortet, A. Chiffaudel, F. Daviaud, and B. Dubrulle, “Experimental evidence of a  
653 phase transition in a closed turbulent flow,” Physical review letters **105**, 214501 (2010).

654 <sup>34</sup>B. Saint-Michel, F. Daviaud, and B. Dubrulle, “A zero-mode mechanism for spontaneous  
655 symmetry breaking in a turbulent von kármán flow,” New Journal of Physics **16**, 013055  
656 (2014).

657 <sup>35</sup>D. Faranda, Y. Sato, B. Saint-Michel, C. Wiertel, V. Padilla, B. Dubrulle, and F. Daviaud,  
658 “Stochastic chaos in a turbulent swirling flow,” Phys. Rev. Lett. **119**, 014502 (2017).

659 <sup>36</sup>B. Dubrulle, F. Daviaud, D. Faranda, L. Marié, and B. Saint-Michel, “How many modes  
660 are needed to predict climate bifurcations? lessons from an experiment,” Nonlinear Pro-  
661 cesses in Geophysics **29**, 17–35 (2022).

662 <sup>37</sup>E. N. Lorenz, “Deterministic nonperiodic flow,” Journal of atmospheric sciences **20**, 130–  
663 141 (1963).

664 <sup>38</sup>J. de Wiljes, A. J. Majda, and I. Horenko, English “An adaptive Markov chain Monte  
665 Carlo approach to time series clustering of processes with regime transition behavior,”  
666 Multiscale modeling & simulation **11**, 415–441 (2013).

667 <sup>39</sup>V. Boyko, S. Krumscheid, and N. Vercauteren, “Statistical learning of non-linear stochas-  
668 tic differential equations from non-stationary time-series using variational clustering,”  
669 arXiv:2102.12395 [math] (2021), arXiv: 2102.12395.